IOP PUBLISHING JOURNAL OF MICROMECHANICS AND MICROENGINEERING
J. Micromech. Microeng. **20** (2010) 000000 (6pp) UNCORRECTED PROOF

Deposition of fibrous nanostructure by ultrafast laser ablation

Amirhossein Tavangar[1], Bo Tan[2] and K Venkatakrishnan[1,3]

[1] Department of Mechanical and Industrial Engineering, Ryerson University, 350 Victoria Street, Toronto, Ontario, M5B 2K3, Canada
[2] Department of Aerospace Engineering, Ryerson University, 350 Victoria Street, Toronto, Ontario, M5B 2K3, Canada

E-mail: venkat@ryerson.ca

Received 22 October 2009, in final form 4 February 2010
Published DD MMM 2010
Online at stacks.iop.org/JMM/20/000000

Abstract
This research work demonstrated that laser-induced reverse transfer (LIRT) can be used for controllable site-specific deposition of fibrous nanostructure. The LIRT method makes it achievable to generate and deposit fibrous nanostructure of a wide variety of materials on a transparent acceptor in a single-step process at an ambient condition. The deposition of fibrous nanostructure was conducted using ultrafast laser ablation of silicon and aluminum targets placed behind a glass acceptor. Femtosecond laser pulses pass through the transparent acceptor and hit the bulk donor. Consequently a mass quantity of nanoparticles ablates from the donor and then aggregates and forms a porous fibrous nanostructure on the transparent acceptor. Our experiments demonstrated that the gap between the target and the glass acceptor was critical in the formation and accumulation of nanofibers and it determines the density of the formed nanostructure. The formation mechanism of the nanostructures can be explained by the well-established theory of vapor condensation within the plume induced by ultrafast laser ablation. Experimental results also show that the length of the nanostructure can be controlled by the gap between the target and glass acceptor. Lastly, energy-dispersive x-ray spectroscopy (EDS) analysis shows the oxygen concentration in the nanofibrous structure which is associated with oxidation of ablated material at ambient atmosphere.

Q1 (Some figures in this article are in colour only in the electronic version)

Introduction

The growth of nano- and poly-crystalline silicon and metallic films on economical substrates like glass has been intensively studied because of their high performance, low cost, copious raw materials and the possibility of being deposited on a large area [1, 2].

Recently, tremendous progress has been achieved in the synthesis of nanoparticles because of the unique physical and chemical properties exhibited when the size of particles are in the order of sub 100 nanometers. Synthesized nanoparticles have various applications in the fabrication of nanodevices in the microelectronic, biomedical, photonic fields, tissue engineering and filtration. Various techniques have been proposed for the generation of nanoparticles. To date, numerous nanofabrication methods, such as electrospinning, phase separation, self-assembly processes, thin film deposition, chemical vapor deposition (CVD), laser ablation, laser chemical vapor deposition (LCVD), are available to synthesize nanomaterials [3].

Among these approaches, the laser ablation technique is desired for its simplicity in equipment configuration and low investment. Laser ablation is widely used in analytic sampling [4], deposition [5] and laser nanofabrication [6–8]. Generally, synthesis of nanoparticles requires the assistance of either a template or a catalyst and more often takes place both at high temperature and in a vacuum environment [9]. Laser-induced forward transfer (LIFT) has been widely studied as a method for direct deposition in predetermined micro-patterns [10–13]. In this method, prior to the laser irradiation a donor thin film is deposited on a transparent support substrate. The ablation of the thin film generates a fast traveling plume that deposits

[3] Author to whom any correspondence should be addressed.

ablated material onto an acceptor substrate which is placed after the donor substrate [14]. Due to the fine spatial resolution of a laser spot, materials can be deposited in desired patterns in micron and sub-micron scale [15, 16]. The LIFT process can be performed in air and at room temperature.

Alternatively, backward-LIFT (laser-induced reverse transfer LIRT) can be used, where the donor substrate is placed after the acceptor substrate along the laser propagation direction. In LIFT, laser ablates the donor thin film from the bottom after transmitting through the transparent support substrate. This imposes limitation on the applicability of LIFT since some materials are not easy to be processed into thin films. Unlike LIFT, LIRT ablates donor material from the front side of the donor substrate. Therefore, donor materials need not to be thin films; instead bulk materials can be used as donors [15]. On the other hand, LIRT requires a transparent acceptor which restrains its applications.

Recently, researchers have begun to examine the potentials of using LIFT for nano-material deposition due to the continuous interest in nanotechnology. For example, Rigout *et al* [16] used a two-step LIFT method to form chain-like silicon nano-wire networks.

In this work, we demonstrated that LIRT can be utilized to generate and deposit metallic and semiconductor nanofibrous structures on a transparent acceptor under ambient conditions. It was found that the distance between the metallic and silicon target and the glass acceptor has a significant influence on the density of fibrous nanostructure. Energy-dispersive x-ray spectroscopy (EDS) analysis was carried out to examine the composition of nanofibrous structure.

Experimental setup and fabrication process

Experiments were conducted with a 515 nm wavelength direct-diode-pumped Yb-doped fiber-amplified ultrafast laser system. The laser gives a maximum output power of 15 W with pulse frequency ranging from 200 kHz to 26 MHz. Due to solid-state operation and high spatial mode quality of fiber lasers, a Yb-doped fiber-oscillator/fiber-amplifier functions under low noise performance. Moreover, parameters of the laser, such as pulse width, repetition rate and total beam power, are computer monitored, which enables a simple interaction with the performed experiments. The pulse width that the laser can produce ranges between 250 fs and 10 ps. The targets are an aluminum sheet and a polished blank silicon wafer with ⟨1 0 0⟩ crystal orientation. They are held stationary and close to a glass acceptor with various spacing in between. The schematic drawing of the experimental setup is shown in figure 1. The experimental setup has been described in detail in [9].

The general laser-induced reverse transfer process is shown schematically in figure 2. The femtosecond laser beam transmits through the transparent acceptor and hits the donor substrate. The plume generated from the donor target surface propagates reversely to the glass acceptor and ejected species agglomerate into nanoparticles which form interwoven nanofibers by further collision.

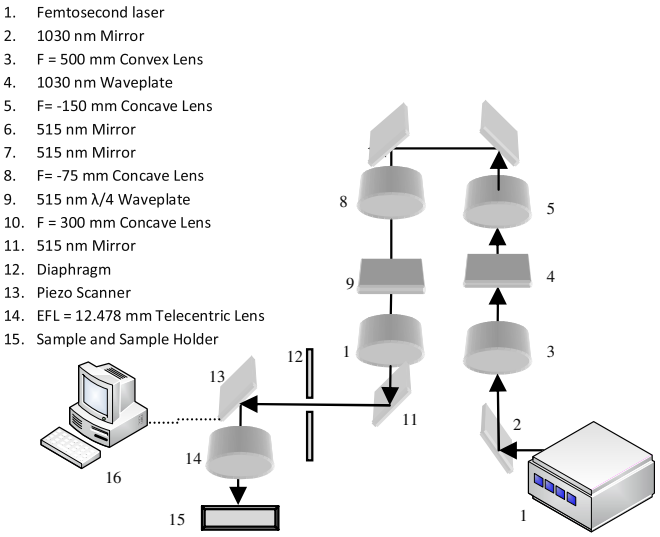

Figure 1. Experimental setup.

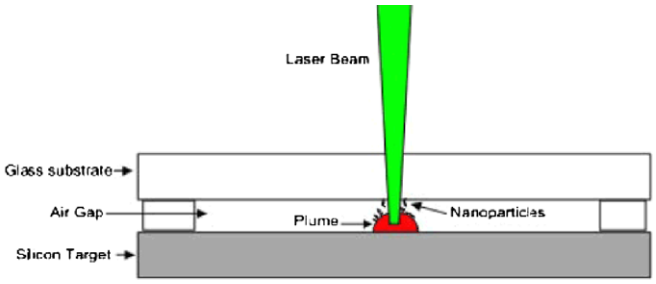

Figure 2. Diagram of laser-induced reverse.

A telecentric lens used to focus the laser beam has 12.478 mm focal length. The theoretical laser minimum spot diameter (D_0) is calculated using $D_0 \approx \frac{1.27\lambda_0 f}{D}$ [18], where λ_0 is the wavelength of the laser, f is the effective focal length of the lens and D denotes the laser beam diameter. The values for these parameters are 12.478 mm, 515 nm and 8 mm, respectively. Thus, the theoretical spot size diameter was calculated to be 1.02 μm. The power of the laser beam varied from 100 mW to 200 mW. Since the frequency used for this experiment was 13 MHz, the laser fluence was computed to be in the range of 0.94–1.88 J cm^{-2}. A pizeoscanner is used to steer the laser beam across the substrate to generate the desired pattern. The scanning speed used for the experiments was 1000 μm s^{-1}. After irradiation, the acceptor substrates were observed using a scanning electronic microscopy (SEM). Energy-dispersive x-ray spectroscopy (EDS) analyses, an integrated feature of a scanning electron microscope, were conducted to examine the composition of nanofibrous structure.

Results and discussions

When the laser intensity surpasses the ablation threshold of a target, the irradiation creates a plasma plume that consists of three propagation fronts of different velocities. The first front is the fastest and it contains vaporized atoms and ions. Due to the small size of atoms and ions, this front is very thin. The second front which starts after the atomic front has lower

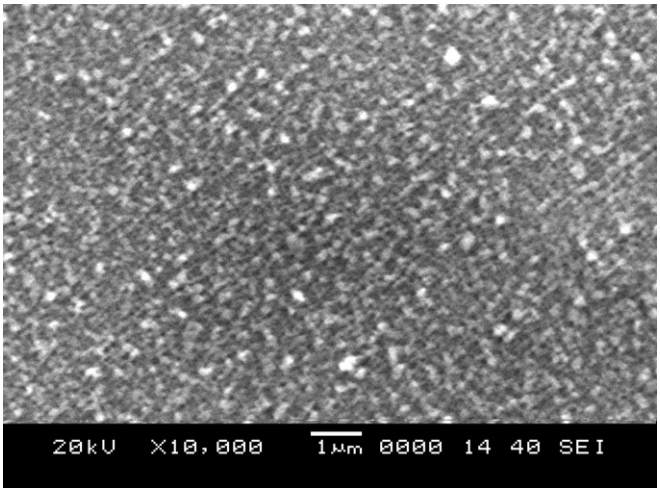

Figure 3. SEM image of aluminum deposition formed by a laser beam of 515 nm wavelength, at a frequency of 13 MHz and a machining velocity of 1000 μm s^{-1}.

velocity and mostly consists of clusters. This front makes the majority of the emitted species [19, 20]. The third front has the longest delay and contains a small amount of molten liquid droplets in micron or submicron size. The bigger the particle size, the shorter it can travel. Therefore, the molten liquid droplets propagate the least distance in comparison with the two other fronts. As the plasma expands outward, the plume's temperature and pressure start to decrease, leading to the nucleation and consequently the growth of nanoparticles [21, 22]. In the case of multiple-pulse irradiation, massive nanoparticle agglomeration takes place if the subsequent pulse arrives before the plume cools below the vaporization point. The agglomerates can be recognized by their chain or web shape. In our case, when a laser pulse is irradiated to the donor substrate, the plasma created on its surface propagates backward at high speed to the transparent acceptor placed close to it. As a result, depending on the distance between the acceptor and the donor substrate, formation and emission of various particle sizes on the acceptor may occur.

In our previous work [7], the synthesis of metallic and silicon fibrous nanostructure on the same substrate using ultrafast laser ablation was demonstrated. It is revealed that the formation of fibrous structure is possible only if the pulse frequency is higher than 1 MHz and the density of nanoparticles and consequently that of the generated nanofibers are maximized at 13 MHz. Thus, the experiments were conducted at a frequency of 13 MHz in order to obtain the highest amount of nanofibers. Here we utilized LIRT to ablate silicon or metallic donors and generate the nanofibrous structure on the transparent acceptors placed in close proximity of the target.

First, the ablation process was performed with a silicon wafer (donor) and a glass acceptor in near contact. Although deposition was presented on the acceptor, no fibrous nanostructures were generated, instead droplets in sub-micron size were observed, as shown in figure 3. Extremely short spacing between the acceptor and the donor restricts the plume expansion and condensation process, resulting in reduction of the nuclei formation onset, hence, leading to the formation of large particles [21, 23]. On the other hand, due to very small separation, molten liquid droplets are able to reach the acceptor surface and deposit.

The role of the substrate distance was thoroughly discussed in LIFT techniques [14, 24–26]. Based on this knowledge, we estimated that a suitable separation of 60 μm should be able to result in nanofiber deposition, taking into account the laser fluence and the target material. This spacing allows more room for plume expansion, leading to a longer plume propagation length. A longer plume length yields a lower concentration of ablated species in the plume which results in smaller clusters [21, 23]. Figure 4 presents the fibrous nanostructures obtained with the 60 μm spacing. However, a small amount of large droplets is still visible from a closeup of the nanostructure, as shown in figure 4(*b*). This suggests that under the current experimental condition, a spacing of 60 μm is not sufficient to completely avoid molten liquid droplet deposition. Direct emission of liquid-phase fragments from the donor surface to the acceptor still occurs on a smaller scale due to the inadequate space.

The experiment was continued with wider gaps at 120, 180 and 240 μm in order to investigate the influence of the target and acceptor distance on the nanofibrous structure. As

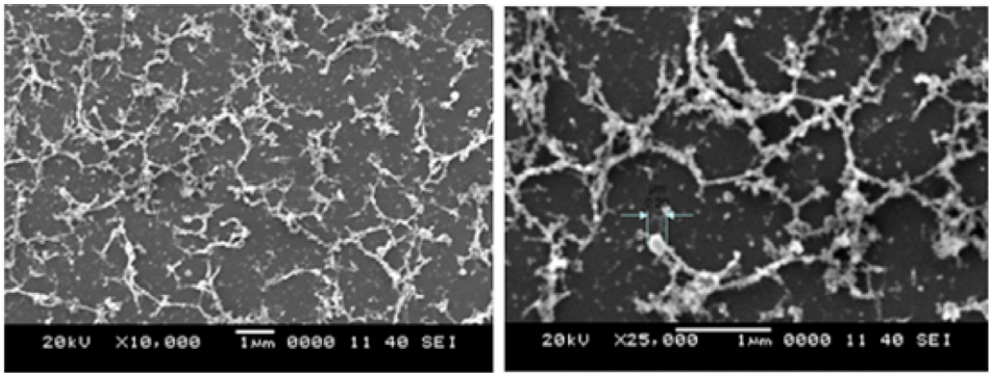

(*a*) (*b*)

Figure 4. SEM image of silicon nanofibers deposited on a glass acceptor with a gap of 60 μm and formed by a laser beam of 515 nm wavelength, at a frequency of 13 MHz and a machining velocity of 1000 μm s^{-1}. At magnification of (*a*) $\times$1000 and (*b*) $\times$25 000.

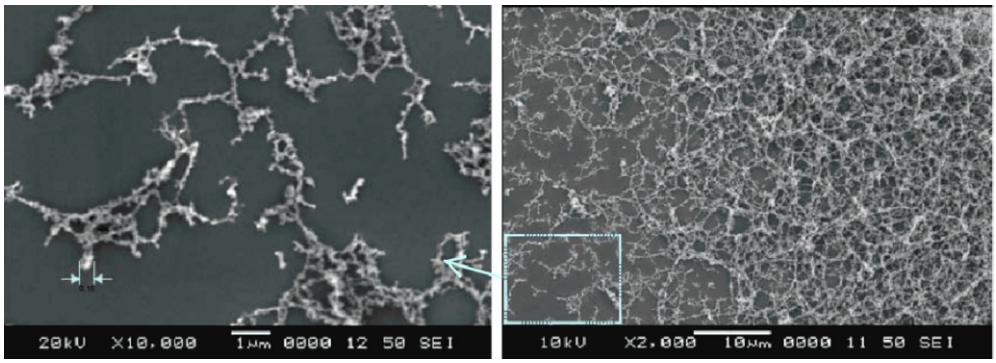

Figure 5. SEM image of silicon nanofibers deposited on a glass substrate with a gap of 120 μm and formed by a laser beam of 515 nm wavelength, at a frequency of 13 MHz and a machining velocity of 1000 μm s^{-1}.

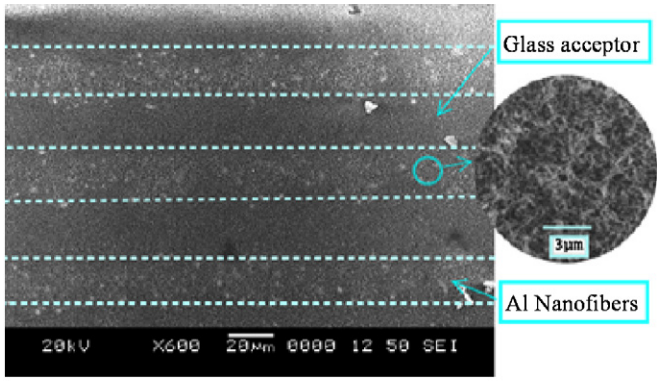

(*a*)

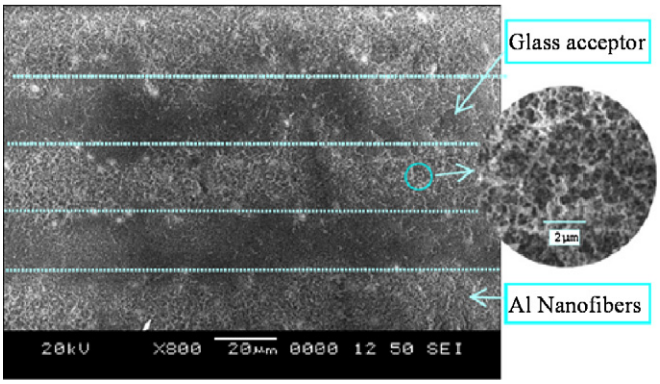

(*b*)

Figure 6. SEM image of aluminum nanofibers deposited on a glass acceptor with (*a*) a gap of 60 μm and (*b*) a gap of 180 μm formed by a laser beam of 515 nm wavelength, at a frequency of 13 MHz and a machining velocity of 1000 μm s^{-1}.

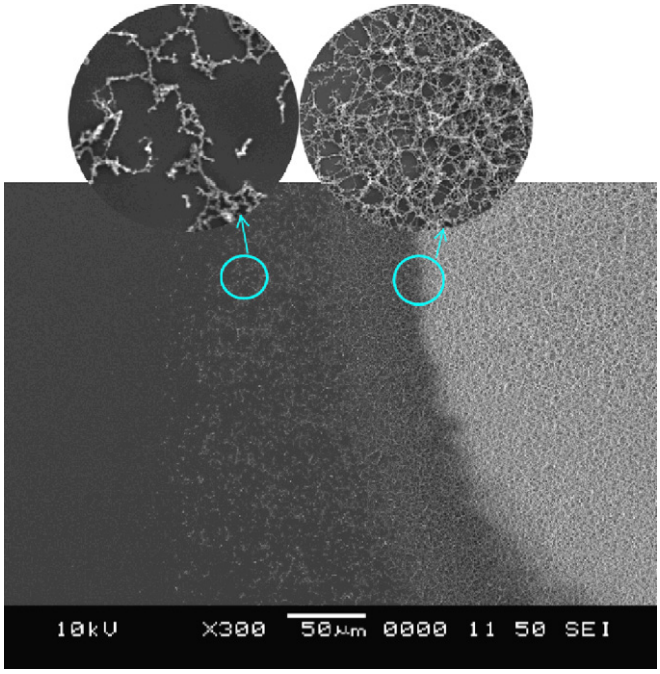

Figure 7. SEM image of three different zones of silicon nanofibers deposited on a glass acceptor with a gap of 120 μm and formed by a laser beam of 515 nm wavelength, at a frequency of 13 MHz and a machining velocity of 1000 μm s^{-1}.

shown in figure 5, the density and length of fibers are more than those on an acceptor with a gap of 60 μm. The average length of nanofibers obtained at the 60 μm gap was in the range of 0.55–0.70 μm whereas it was about 1.06–1.18 μm for those obtained at the 120 μm gap. Comparing figures 4(*a*) and 5, we found that the large droplets diminished in size and amount. Besides, as the gap between the target and the acceptor increased, deposited nanofibers became thinner.

The experiment was repeated with other target materials such as aluminum and graphite. It was found that, the aggregates can be deposited from metals, carbon and semiconductors. Alloy targets composed of these elements were also found to generate the fibrous nanostructure by ultrafast laser irradiation.

Figure 6 gives nanofibers that were generated in parallel lines. It demonstrates that deposition of nanofibers can be carried out at specific sites. Comparing figures 6(*a*) and (*b*), it can be seen that the density of nanofibers increased with the increase in the gap between the glass acceptor and the donor.

Figure 7 shows a spot ablated with a stationary laser beam. Nanofiber density is the maximum at the center of the spot and decreases with the increase in the radial distance from the center of the laser spot. At larger distances, the density of the nanofibers falls dramatically. This observation agrees well with the previous study on spectroscopy of laser-ablated

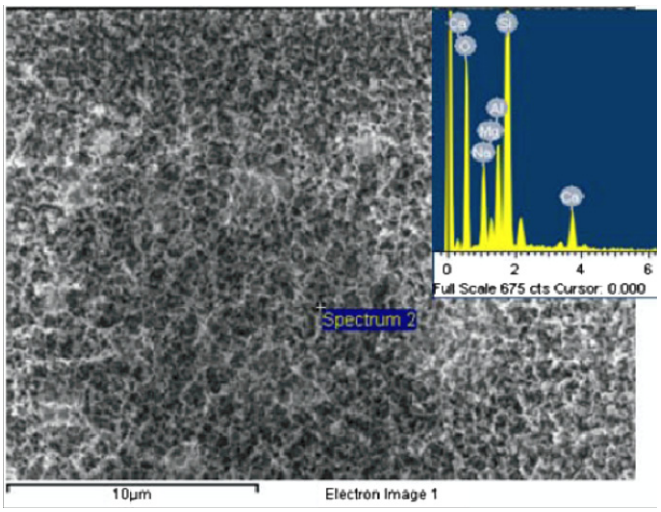

Figure 8. Energy-dispersive x-ray spectroscopy (EDS) analysis of aluminum oxide nanofibers deposited on a glass acceptor.

silicon plasma related to nanoparticle formation [27]. The spatial dependence shows the reduction in temperature and density with the increase in distance. The high plasma pressure causes a lateral plasma compression wave, leading to a change in energy distribution on the target, which explains the density of variety of deposition along the radial direction [27].

In order to examine the composition of nanofibrous structure, energy-dispersive x-ray spectroscopy (EDS) analysis was carried out. As depicted in figure 8, EDS analysis of aluminum nanofibrous structure on the glass acceptor showed Si, Ca and O together with aluminum. To investigate whether these elements belong to the glass acceptor or the nanofibrous structure, EDS analyses of the glass acceptor with and without nanofibrous structure were compared. By comparison between those results, it was concluded that only oxygen concentration is higher in the nanofibrous structure and other elements belonged to the glass acceptor. Since the LIRT process is performed at atmospheric ambient, oxidation of ablated nanoparticles occurs, which results in the generation of the metallic or silicon oxide nanofibrous structure. In order to confirm the nanofiber composition and precise measurement of the oxygen level, EDS analysis was obtained for silicon nanofibers which were directly generated on the pure Si substrate. As shown in figure 9, for Si nanofibers, the presence of O along with Si agrees with Al EDS analysis.

Conclusion

In this paper, we have demonstrated the deposition of metallic and semiconductor fibrous nanostructure on a glass acceptor using femtosecond laser-induced reverse transfer at an ambient condition. It was found that the gap between the glass acceptor and the target plays a crucial role in the nanostructure formation and the density of nanofiber accumulation. Experimental results also show that size, length, density of aggregates and location of growth can be controlled by laser parameters under an ambient condition. Finally, EDS results illustrate the oxygen concentration in the nanofibrous structure, which is ascribed to the oxidation of ablated material due to the presence of oxygen in an ambient atmosphere. The precise controllability of this fibrous nanostructure deposition will extend the application

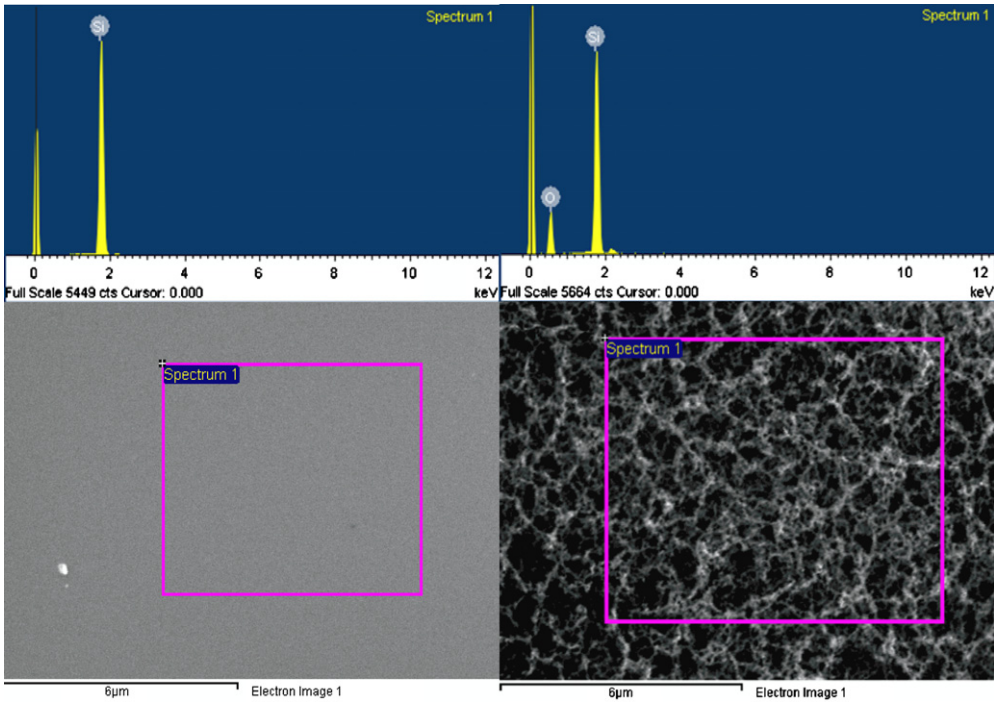

Figure 9. Energy-dispersive x-ray spectroscopy (EDS) analysis of pure Si (left) and silicon oxide nanofibers deposited on a Si substrate (right).

of this invention. Generation and deposition of nanofibrous structure is completed in a single step at an ambient condition. This method may find wide applications. For instance, it can be used to synthesize nano-composite, fabricate porous filters, construct tissue scaffolds and generate electromagnetic radiation shields for nano-devices, just to name a few.

Q2

References

[1] Fujiwara H, Kondo M and Mastuda A 2003 *J. Appl. Phys.* **93** 2400–9
[2] Saha S C, Rath J K, Kshirsagar S T and Ray S 1997 *J. Phys.* D **30** 2686–92
[3] Zhang L. and Webster T. J. 2008 *Nano Today* **4** 66–80
[4] Bogaerts A, Chen Z, Gijbels R and Vertes A 2003 *Spectrochim. Acta* **58** 1867–93
[5] Chrisey D B, Pique A, McGill R A, Horwitz J S, Ringeisen B R, Bubb D M and Wu P K 2003 *Chem. Rev.* **103** 553–76
[6] Meijer J, Du K, Gillner A, Hoffmann D, Kovalenko V S, Masuzawa T, Ostendorf A, Poprawe R and Schul W 2002 *CIRP Ann. STC* **50** 531–50
[7] Venkatakrishnan K and Tan B 2009 *Opt. Express* **17** 1064–9
[8] Senadheera S, Tan B and Venkatakrishnan K 2009 *Nanotechnology* **1** 590763
[9] Tan B, Dalili A and Venkatakrishnan K 2009 *J. Appl. Phys.* A **95** 537–45
[10] Yamada H, Sano T, Nakayama T and Miyamoto I 2002 *Appl. Surf. Sci.* **411** 197–8
[11] Zergioti I 2005 *Appl. Phys. Lett.* **86** 163902
[12] Papantonakis M R and Haglund Jr R F 2004 *Appl. Phys.* A **79** 1687–94
[13] Tan B, Venkatakrishnan K and Tok K G 2003 *Appl. Surf. Sci.* **207** 365–71
[14] Veiko V P and Metev S M 1995 (Heidelberg: Springer) Q3
[15] kuznetsov A I, Koch J and Chichkov B N 2009 *Opt. Express* **17** 18820–5
[16] Rigout M L A, Niu H, Qin C, Zhang L, Li C, Bai X and Fan N 2008 *Nanotechnology* **19** 245303
[17] Veiko V P, Shakhno E A, Smirnov V N, Miaskovski A M and Nikishin G D 2006 *Laser Part Beams* **24** 203–9 Q4
[18] Venkatakrishnan K, Tan B, Stanley P, Lim L E N and Ngoi B K A 2002 *Opt. Eng.* **41** 1441–5
[19] Perriere J, Boulmer-Leborgne C, Benzerga R and Tricot S 2007 *Appl. Phys.* B **40** 7069–76
[20] Zhigilei L V 2003 *Appl. Phys.* A **76** 339–50
[21] khang Y and Lee J 2009 *J. Nanopart. Res.* DOI:10.1007/s11051-009-9669-z
[22] Lescoute E, Hallo L, Hébert D, Chimier B, Etchessahar B, Tikhonchuk V T, Chevalier J M and Combis P 2008 *Phys. Plasmas* **15** 063507–18
[23] Franklin S R and Thareja R K 2005 *Appl. Phys.* **97** 123303–8
[24] Bera S, Sabbah A J, Yarbrough J M, Allen C G, Winters Beau, Durfee C G and Squier J A 2007 *Appl. Opt.* **46** Q5
[25] Sano T, Yamada H, Nakayama T and Miyamoto I 2002 *Appl. Surf. Sci.* **186** 221–6
[26] Kántor Z, Tóth Z and Szörényi T 1992 *Appl. Phys.* A **54** 170–5
[27] Narayanan V and Thareja R K 2004 *Appl. Surf. Sci.* **222** 382–93

QUERIES

Page 1

Q1

Author: Please be aware that the colour figures in this article will only appear in colour in the Web version. If you require colour in the printed journal and have not previously arranged it, please contact the Production Editor now.

Page 6

Q2

Author: Please check the details for any journal references that do not have a blue link as they may contain some incorrect information. Pale purple links are used for references to arXiv e-prints.

Q3

Author: Please provide missing information in reference [14].

Q4

Author: Reference [17] is not cited in the text.

Q5

Author: Please provide page number(s) in reference [24].